Chinese Chemical Letters 35 (2024) 109545

Contents lists available at ScienceDirect

Chinese Chemical Letters

journal homepage: www.elsevier.com/locate/cclet

The synergistic effect of A-site cation engineering and phase regulation enables efficient and stable Ruddlesden-Popper perovskite solar cells

Rui Liu[a], Yue Yu[a], Lu Deng[a], Maoxia Xu[a], Haorong Ren[a], Wenjie Luo[a], Xudong Cai[a], Zhenyu Li[a,b,*], Jingyu Chen[a,b,*], Hua Yu[c,*]

[a] The Center of Functional Materials for Working Fluids of Oil and Gas Field, School of New Energy and Materials, Southwest Petroleum University, Chengdu 610500, China

[b] Sichuan Engineering Technology Research Center of Basalt Fiber Composites Development and Application, State Key Laboratory of Oil and Gas Reservoir Geology and Exploitation, Southwest Petroleum University, Chengdu 610500, China

[c] School of Physical Sciences, Great Bay University, Dongguan 510799, China

ARTICLE INFO

Article history:
Received 20 December 2023
Revised 15 January 2024
Accepted 17 January 2024
Available online 23 January 2024

Keywords:
Phase control
Layered perovskite
Synergistic effect
Low *n* phase
Stability

ABSTRACT

$BA_2(MA)_{n-1}Pb_nI_{3n+1}$ series low-dimensional (2D) perovskites have been widely investigated for their remarkable environmental stability, but still suffer the poor light absorption and disordered phase distribution, hindering their practical applications. In this work, we combine the introduction of FA and the addition of $PbCl_2$ to optimize the film quality, strengthen the light absorption, regulate internal phase distribution, and promote carrier transport inside 2D perovskite films. The incorporation of FA promotes sufficient light absorption and improve the film crystallinity. Furthermore, the addition of $PbCl_2$ eliminates the low *n* phase ($n=1$) and suppresses the forming of the low *n* phase of $n=2$, enhancing the film conductivity and diminishing carrier recombination. The synergistic of A-site cation engineering and phase manipulation achieves a high efficiency of 16.48%. Importantly, the synergistic prepared perovskite film does not show any changes after 60 days in the air with an average humidity of 57% ± 3%, and the corresponding solar cell maintains 85% of the original efficiency after more than 800 h, demonstrating remarkable environmental stability. The results indicate that the synergistic of A-site cation engineering and phase manipulation is promising for producing superior efficiency, along with satisfying humidity stability.

Past decade has witnessed an earthshaking efficiency progress for 3D perovskites [1,2]. However, because the poor chemical stability of the 3D perovskite, it is easy to degrade under environmental conditions such as, oxygen, humidity and high temperature, which greatly hinders their commercialization process [3,4]. 2D metal halide perovskites presenting remarkable environmental stability suitable for practical application have given rise to tremendous interest and making this magic material a rising star in photovoltaic technologies.

Depending on the type of introduced organic spacer cations, 2D perovskites can form Ruddlesden-Popper (RP), Dion-Jacobson (DJ), and alternating cations interlayer (ACI) phase three different types [5]. Among them, 2D RP perovskites of $BA_2(MA)_{n-1}Pb_nI_{3n+1}$ series (BA series) are considered to be the most promising and potential layered materials due to their superior environmental stability and favorable reproducibility [5,6]. The PCE of BA series materials ($n \leq 5$) has experienced a remarkable increase in recent years [7,8]. However, BA series 2D perovskite materials encounter two challenges that affect their device performance. One is inefficient light absorption and the other is the presence of low *n* phases [9,10]. The low *n* phases are poorly conductive and act as a carrier trap, resulting in lower efficiency devices [9,11]. For the issue of inefficient light absorption, Chen *et al.* reported double A-site cation 2D perovskite for the first time, achieving an ideal band gap of 1.51 eV [12]. Unfortunately, they achieved only 6.88% PCE due to poor film quality. Later, Shao *et al.* incorporated guanidinium (GA^+) into PEA-based RP 2D perovskite fabricating a mixed bulky $(PEA,GA)_2MA_4Pb_5I_{16}$ 2D perovskite [13]. They found that the incorporating GA^+ not only enhanced the light absorption of 2D perovskite, but also promoted the carrier transport inside the 2D perovskite

* Corresponding authors.
E-mail addresses: zhenyu.li@swpu.edu.cn (Z. Li), jingyu_chencn@hotmail.com (J. Chen), yuhua@gbu.edu.cn (H. Yu).

https://doi.org/10.1016/j.cclet.2024.109545
1001-8417/

film. Although many other efforts have been made to reduce the band gap of 2D RP perovskites, the relatively low efficiency produced by inappropriate n value choosing has limited their further development [14,15]. To the issue of disordered phase distribution, Lee *et al*. found that addition of DMSO in DMF solvent can reduce the intensity of low n phases, thereby reducing carrier recombination centers and improving device performance [11]. Then, Xu *et al*. found 2D perovskite (BA, OA)$_2$(MA, FA)$_2$Pb$_n$I$_{3n+1}$ ($n=4$) with OA cation exhibits enhanced charge transport due to inhibition of low n phases [16]. To realize better carrier transport, in 2020, Liu *et al.* reported a synergistic effect and found optimization of solvent ratio and substrate preheating temperature can gradually reduce the intensity of low n phases [17]. Though better charge transport was achieved within 2D perovskites through regulate the phase distribution, the efficiency is still far from satisfactory since the low n phases is only suppressed rather than eliminated.

In this work, we combine the introduction of FA and the addition of $PbCl_2$ fabricated FA/MA mixed $BA_2(MA_{1-x}FA_x)_4Pb_5I_{3n+1}$ ($n=5$) layered perovskites. This method avoids the issue of poor film quality caused by inappropriate n value selection and completely eliminates the existence of low n phase of $n=1$. In comparison with the FA-free 2D perovskite film, the optimal FA-based film exhibits improved crystallinity and enhanced light absorption, achieving a higher J_{SC} of 20.01 mA/cm^2 than the FA-free sample of 17.86 mA/cm^2. After further addition of $PbCl_2$ in the optimal FA/MA mixed precursor solution, we observed that the low n phase of $n=1$ was fully eliminated and the low n phase of $n=2$ was noticeably suppressed. In addition, the $PbCl_2$-added 2D perovskite exhibits micron-level grain size (1.83 μm) with enhanced film crystallinity. Importantly, the $PbCl_2$-added 2D perovskite film displays higher surface contact potential, reduced trap density, and superior carrier transport, thus a high PCE of 16.48%. The optimal $PbCl_2$-added $BA_2(MA_{0.95}FA_{0.05})_4Pb_5I_{16}$ film and device also display superior environmental stability after storage in an average humidity of 57% ± 3%.

The $BA_2(MA)_4Pb_5I_{16}$ (control) film was prepared by one-step hot-casting method using (BAI), methyl ammonium iodide (MAI) and lead iodide (PbI_2) as raw materials and DMF/DMSO as a binary solvent. As discussed in the introduction, cation FA was employed to partially replace cation MA in $BA_2(MA)_4Pb_5I_{16}$ material aiming to obtain a band gap moderate mixed A site cation 2D perovskites. The amount of FA is determined according to the components of $BA_2(MA_{1-x}FA_x)_4Pb_5I_{16}$ ($x=0$, 0.05, 0.10, 0.20, 0.40). For the prepared $BA_2(MA_{1-x}FA_x)_4Pb_5I_{16}$ series, some targeted characterizations were conducted to investigate the effect of FA introduction on the 2D perovskite films.

First, we carried out X-ray diffraction (XRD) and ultraviolet absorption spectrum (UV) to investigate the structure variation and light absorption case upon the introduction of cation FA. Fig. 1a represents XRD patterns of different amount of FA introduced 2D perovskite films. All films display (111) and (202) character diffraction peaks of 2D perovskite in 14.1° and 28.3° [19,20]. After the introduction of FA, the diffraction peak shifted to the lower diffraction angles, indicating that FA/MA layered 2D perovskite was successfully processed [10,21]. It is worth mentioning that the full-width at half-maximum (FWHM) value of (111) and (202) two diffraction peaks gradually decrease as the increasing of FA ratio (Fig. 1b), confirming increased crystal size and improved crystallinity. Note that low angle diffraction peak appeared when the FA content was higher than 0.05. We speculate that this could be ascribed to the formation of $BA_2FAPb_2I_4$ (low n phase) perovskite owing excess FA introduction. The low n phase has the drawbacks of a large band gap, poor conductivity, and mismatched energy band structure [5,22,23], which is not conducive to device performance. We observed that after the introduction of FA, the absorption of 2D perovskite film enhanced first and then attenuated

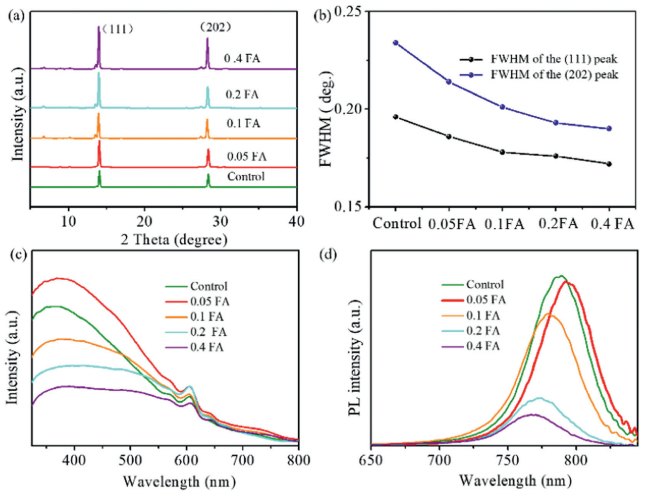

Fig. 1. (a) XRD diffraction results of different FA content-based-2D perovskite films. (b) The (111) and (202) half-peak width values of 2D perovskite films at different contents of FA ratios. (c, d). UV–vis absorption and PL spectra of different FA content based-2D perovskite films.

(Fig. 1c). The optimal FA/MA mixed 2D perovskite film (0.05 FA) exhibits absorption edge red-shifts in comparison with the control film, from 646 nm to 659 nm. This result demonstrates that the addition of FA indeed reduced the optical band gap and enhanced the light absorption. The PL results of different FA contents introduced 2D perovskite films are shown in Fig. 1d. As increasing FA ratio from 0.05 to 0.40, PL peak displayed red-shift (0.05FA) and then blue-shift (FA > 0.05), which is due to the formation of low n phase of 2D perovskites after FA content was higher than 5%. The performance statistics distribution for different amounts of FA-introduced devices is shown in Fig. S1a (Supporting information). It is observed that the optimal FA replacement amount is 0.05, and the device efficiency decreases when it is higher than 0.05. The corresponding *J-V* curves and device parameters are displayed in Fig. S1b and Table S1 (Supporting information). The average value of the J_{SC} increased from 17.76 mA/cm^2 to 19.70 mA/cm^2 for FA-free and FA-introduced 2D perovskite devices. The performance improvement after the introducing cation FA may arise from the enhancement of light absorption due to the extending of the absorption range.

We further introduced $PbCl_2$ to regulate the crystallization process of 2D perovskite to improve the film quality and device performance. Fig. 2a exhibits the PL spectra of 2D perovskite films after the addition of different molar ratios of $PbCl_2$. The resultant 2D perovskite displays multiple perovskite phases, indicating a multi-phase mixed structure. Meanwhile, we observed that after the addition of $PbCl_2$, the peak intensity of the 3D perovskite gradually decreases, revealing the holes and electrons are easily separated and extracted in $PbCl_2$-introduced 2D perovskite films [24,25]. It is worth noting that when the PL spectrum is locally amplified (500–675 nm), we found that the addition of 1.5 mol% $PbCl_2$ ($PbCl_2$-added) eliminated the low n phase of $n=1$ and suppressed the formation of low n phase of $n=2$ (Fig. 2b). This result demonstrates that the addition of $PbCl_2$ effectively regulated the crystallization growth process and crystallization kinetics of layered low dimensional perovskite. Based on the above results, we propose the schematic diagrams (Fig. 2c) of the phase distribution of $PbCl_2$-free and $PbCl_2$-added perovskite. Owing to containing fewer low-n phases, $PbCl_2$-added 2D perovskite promotes internal carrier transport, which is conducive to improving device performance [11,16].

After studying the phase distribution of 2D perovskite at different molar ratios of $PbCl_2$, atomic force microscope (AFM) was

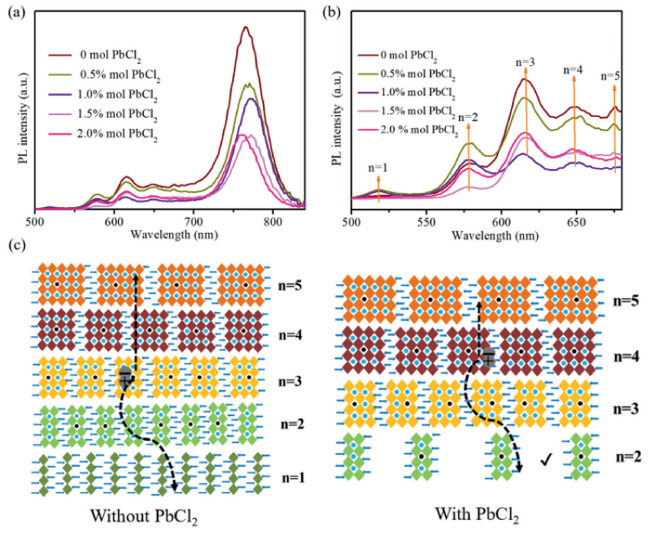

Fig. 2. (a) PL spectra of 2D perovskite films at different molar ratios of $PbCl_2$ (excited from perovskite back side). (b) Locally amplified PL results (500–675 nm). (c) Phase distribution schematic diagrams of $PbCl_2$-free and $PbCl_2$-added 2D perovskites.

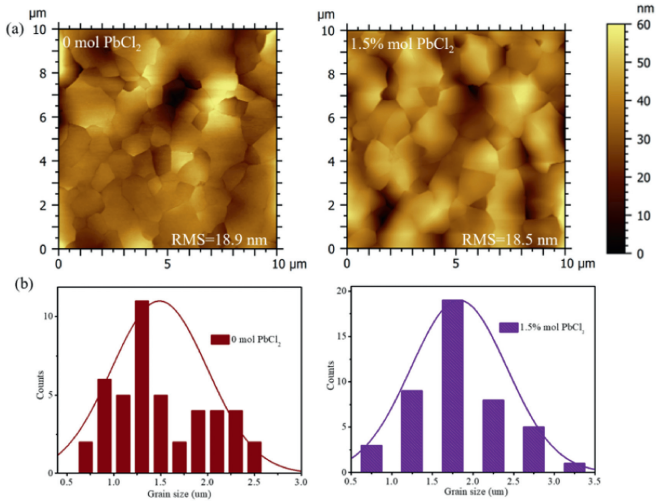

Fig. 3. (a) AFM images of $PbCl_2$-free and $PbCl_2$-added 2D perovskites. (b) 2D perovskite grain size statistics based on AFM results.

performed for $PbCl_2$-free and $PbCl_2$-added layered low dimensional perovskite films (Fig. 3a). The $PbCl_2$-free 2D perovskite film shows small grain size and uneven grain size distribution, with a root-mean-square roughness (RMS) of 18.9 nm. However, the $PbCl_2$-added 2D perovskite exhibits larger grain size and uniform grain size distribution, with an RMS value of 18.5 nm. This result demonstrates that the introduction of $PbCl_2$ can delay the precipitation of FA/MA mixed supersaturated precursor solution, and is conducive to forming crystal grains with larger size due to the decreasing of nucleation sites [26]. Meanwhile, this result also verifies again that the addition of $PbCl_2$ indeed regulates the crystallization growth process and crystallization kinetics of 2D perovskite. Fig. 3b displays the grain size statistics of $PbCl_2$-free and $PbCl_2$-added 2D perovskite films. The $PbCl_2$-added 2D perovskite has an average grain size of 1.83 μm dramatically larger than the $PbCl_2$-free sample, which can be seen more clearly from the supplementary material (Fig. S2 in Supporting information). The increased grain size implies improved crystallinity and reduced grain boundary of FA/MA mixed 2D perovskite, which can greatly promote carrier transport within the 2D perovskite [27]. Fig. S3 (Supporting information) exhibits corresponding SEM images, both the $PbCl_2$-free and $PbCl_2$-added film showed uniform and complete surface coverage.

To gain a deeper understanding of the underlying physics behind charge carrier transport in $PbCl_2$-added 2D perovskites, the photoelectric properties of the $PbCl_2$-free and $PbCl_2$-added perovskite films were systematically characterized. Figs. 4a and b exhibit the kelvin probe force microscopy (KPFM) images of the $PbCl_2$-free and $PbCl_2$-added 2D perovskites. Potential variations from ≈ −322 mV to −94 mV were observed for $PbCl_2$-free 2D perovskite film, while it was enhanced to ≈−0.084 mV to 0.0967 mV for $PbCl_2$-added perovskite film. Meanwhile, the surface potential of $PbCl_2$-added 2D perovskite films exhibits enhanced uniformity compared to those $PbCl_2$-free samples (Fig. 4c). In addition, after addition of $PbCl_2$, the average values of the surface potentials increased from −207 mV to 11.2 mV, indicating that 1.5 mol% $PbCl_2$ addition promotes the separation and transportation of charge carriers within the perovskite film [28]. Time-resolved photoluminescence (TRPL) spectra (Fig. 4d) reveal that $PbCl_2$-added 2D perovskite film displays a longer average carrier lifetime of $\tau = 11.72$ ns than $\tau = 3.80$ ns for $PbCl_2$-free sample, specific attenuation parameters τ_1 and τ_2 are listed in Table S2 (Supporting information). Enhanced carrier lifetime suggested that the addition of $PbCl_2$ suppressed carrier recombination and improved the film quality [29,30]. Meanwhile, alternating current impedance spectroscopy measurements are conducted, corresponding Nyquist plots results shown in Fig. 4e. The recombination resistance (R_{rec}) was dramatically increased from 1433 Ω (without $PbCl_2$) to 1837 Ω for the $PbCl_2$-added device implying that the addition of $PbCl_2$ inhibit carrier recombination inside the perovskite film [31], specific resistance parameters are shown in Table S3 (Supporting information). Based on the above analysis, we can conclude that the introduction of $PbCl_2$ promotes carrier transport, reduces defect density, and suppresses carrier recombination within the perovskite film. These results demonstrate that $PbCl_2$ is a resultful additive to improve the quality of layered low dimensional perovskite films.

To further investigate the charge-carrier physics in $PbCl_2$-added 2D perovskite films, incident light intensity dependence of V_{OC}, dark *J-V* curves, and motte-schottky curves were performed. Light intensity-dependent V_{OC} is demonstrated to correlate with the charge recombination loss in the usage of the devices [32]. As shown in Fig. 5a, according to the fitting result, the $PbCl_2$-added solar cell has a V_{OC} *versus* P_{light} slope of $0.947kT/q$, which is much smaller than the $PbCl_2$-free sample of $1.16kT/q$, where k is Boltzmann's constant, T is temperature, and q is elementary charge. This result suggests that trap-assisted recombination is noticeably suppressed in the $PbCl_2$-added devices [33]. Fig. 5b is the dark *J-V* curves of 2D perovskite devices. The $PbCl_2$-added device produces a lower dark current of 2.74×10^{-3} mA/cm^2 than the $PbCl_2$-free one (2.21×10^{-2} mA/cm^2), indicating less trap states in the $PbCl_2$-added devices [34]. Space-charge-limited current (SCLC) method was used to quantitatively describe the trap density within the 2D perovskite for $PbCl_2$-free and $PbCl_2$-added hole-only devices (ITO/NiOx/2D perovskite/Spiro-OMeTAD/Ag). The fitting results are shown in Fig. 5c. According to the formula of $N_{trap} = 2\varepsilon\varepsilon_0 V_{TFL}/qL^2$ [35], where ε_r is the relative dielectric constant ($\varepsilon_r = 25$), ε_0 is the vacuum permittivity, q is the elemental charge, and L is the thickness of the photo-absorber layer (600 nm), the $PbCl_2$-added device delivers a lower trap density of 2.05×10^{15} cm^{-3} than the $PbCl_2$-free sample of 3.71×10^{15} cm^{-3}. This result suggested that the addition of $PbCl_2$ can effectively reduce the trap density within the perovskite films, thus reducing non-radiative recombination and improving film quality. To further investigate the effect of $PbCl_2$ addition on the carrier transport, we conducted the Motte-Schottky curve (Fig. 5d). The $PbCl_2$-added device generates a built-in electric field (V_{bi}) of 0.814 V noticeably higher than the $PbCl_2$-free sample

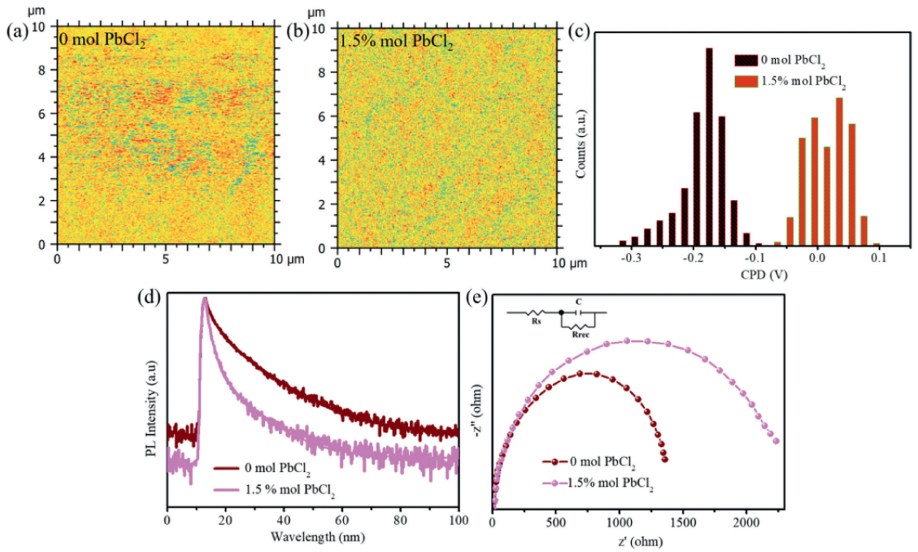

Fig. 4. (a, b) KPFM images of $PbCl_2$-free and $PbCl_2$-added perovskite film. (c) Surface contact potential differences (CPD) distribution statistics. (d, e) Corresponding TRPL spectra and Nyquist plots.

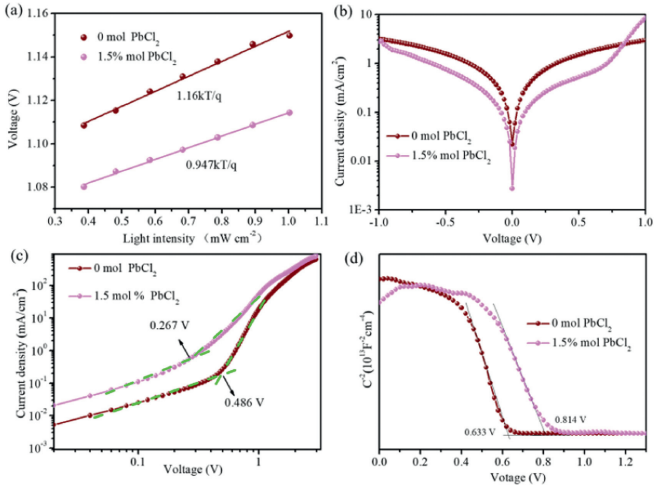

Fig. 5. (a) Incident light intensity dependence of V_{OC} for $PbCl_2$-free and $PbCl_2$-added devices. (b, c) Dark *J-V* curves for $PbCl_2$-free and $PbCl_2$-added devices. (d) Corresponding Mott-Schottky plots.

of 0.633 V, which indicates that the addition of $PbCl_2$ drives the separation and transport of photogenerated carriers [18]. These results indicate that the addition of $PbCl_2$ efficaciously reduces the defect density in perovskite films, thereby facilitating carrier separation and transport within the films.

To verify the photovoltaic performance of $PbCl_2$-free and $PbCl_2$-added devices, inverted planar PSCs were fabricated with a device architecture of indium tin oxide (ITO) /NiO_x/2D perovskite /PCBM/BCP/Ag. Fig. S4 (Supporting information) exhibits the efficiency distribution diagram of perovskite cells with different content of $PbCl_2$. After adding 1.5 mol% $PbCl_2$, 2D perovskite showed the optimal efficiency. Table 1 displays the champion and average (Ave) device parameters of $PbCl_2$-free and $PbCl_2$-added solar cells (forward scan). The $PbCl_2$-free sample shows an average PCE of 14.77%, V_{oc} of 1.11 V, J_{SC} of 19.41 mA/cm^2, FF of 69.8%, a highest V_{oc} of 1.16 V, FF of 75.53%, a decent PCE of 15.72%. After addition of 1.5 mol% $PbCl_2$ into the optimal FA-based 2D perovskite precursor, the average PCE was enhanced to 15.46%, FF to 70.5%, achieving a highest PCE of 16.48%. The enhanced PCE performance

Table 1
Device parameters of $PbCl_2$-free and $PbCl_2$-added solar cells.

$PbCl_2$-added	Device parameter	V_{OC} (V)	J_{SC} (mA/cm^2)	PCE (%)	FF (%)
0 mol%	Champ	1.16	17.91	15.72	75.53
	Ave	1.11	19.41	14.77	69.8
1.5 mol%	Champ	1.16	19.01	16.48	74.5
	Ave	1.12	19.72	15.46	70.5

is ascribed to the effective phase regulation of 2D perovskite by the addition of $PbCl_2$. Fig. 6a exhibits the EQE spectrum of the $PbCl_2$-free and $PbCl_2$-added champion devices. The J_{SC} integrated from the incident photon to current conversion efficiency (IPCE) spectra was 17.41 mA/cm^2 and 18.32 mA/cm^2 for the $PbCl_2$-free and $PbCl_2$-added solar cell, analogously matching (<5% discrepancy) well with the value derived from the *J-V* curves (Fig. 6b). This result confirms the increased device performance, because of the effective phase regulation and improved charge transport.

To verify the impact of chloride additive on the stability of layered 2D perovskite, the fabricated film and unencapsulated 2D photovoltaic devices were placed in a harsh atmosphere with an average humidity of 57% ± 3%. For the $PbCl_2$-free sample, the peak intensity of (111) and (202) diffraction planes markedly decreased after 60 days of storage (Fig. 6c), which reflected poor humidity stability. Nevertheless, as shown in Fig. 6d, the $PbCl_2$-added 2D perovskite film displays completely unchanged peak strength. Meanwhile, as shown in Fig. 6e, the $PbCl_2$-added 2D perovskite solar cell exhibits relatively higher moisture stability in comparison with the $PbCl_2$-free sample after storage of more than 800 h in air. These results show that the addition of $PbCl_2$ significantly enhances the humidity resistance of layered perovskite films and devices, which may be due to the reduction of defects and the improvement of film quality after the addition of $PbCl_2$. We tested the champion $PbCl_2$-added 2D perovskite device from different scanning directions (Fig. S5 in Supporting information). The resultant $PbCl_2$-added 2D perovskite solar cell displays ignorable hysteresis (less than 5%). The improved stability and negligible hysteresis confirmed again that the addition of $PbCl_2$ has a benign effect on 2D perovskite films, which is conducive to improving the device performance.

Mix cation $BA_2(MA_{0.95}FA_{0.05})_4Pb_5I_{16}$ perovskite films were successfully prepared by introducing cation FA to replace cation MA.

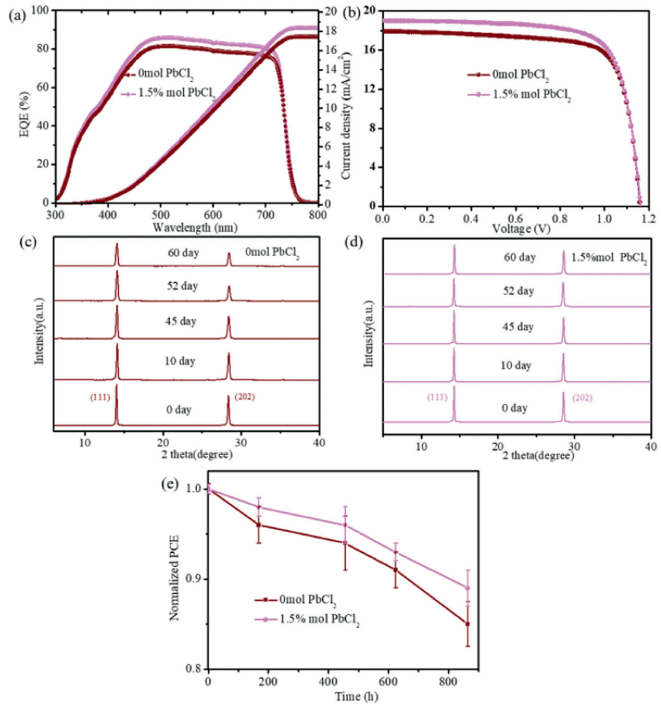

Fig. 6. (a) EQE spectrum of the $PbCl_2$-free and $PbCl_2$-added champion devices. (b) Corresponding *J-V* curves (forward scan). (c, d) XRD aging test results of $PbCl_2$-free and $PbCl_2$-added layered perovskite films at an average humidity of 57% ± 3%. (e) Corresponding photovoltaic device humidity resistance results.

The incorporation of FA strengthened the light absorption range and enhanced the crystallinity of 2D perovskite contributing to notably improved J_{SC}. After further introduction of $PbCl_2$, the low n phase of $n=1$ was eliminated and the low n phase of $n=2$ was notably suppressed. Meanwhile, the addition of $PbCl_2$ promoted the formation of 2D perovskite films with large grain size and less defect density, which greatly facilitated the carrier transport within the 2D perovskite film. Importantly, the $PbCl_2$-added layered perovskite film and device show significantly enhanced moisture stability in contrast to the $PbCl_2$-free sample. The synergistic effect of A-site cation engineering and phase regulation achieves an impressive PCE of 16.48%. Our results highlight a promising future of efficient and sTable 2D PSCs toward commercialization.

Declaration of competing interest

The authors declare no conflict of interest.

Acknowledgments

This work financially supported by the Chengdu Science and Technology Program (No. 2021GH0200032HZ), and Sichuan Engineering Technology Research Center of Basalt Fiber Composites Development and Application (No. 2022SCXWYXWFC006), and Natural Science Foundation of Sichuan Province (No. 2022NSFSC0356).

Supplementary materials

Supplementary material associated with this article can be found, in the online version, at doi:10.1016/j.cclet.2024.109545.

References

[1] J. Xu, J. Chen, S. Chen, et al., Chem. Eng. J. 453 (2023) 139790.
[2] J. Xu, H. Chen, L. Grater, et al., Nat. Mater. 23 (2023) 23450.
[3] H. Peng, D. Li, Z. Li, et al., Nanomicro Lett 15 (2023) 91.
[4] H. Zheng, D. Liu, Y. Wang, et al., Chem. Eng. J. 389 (2020) 124266.
[5] R. Liu, X. Hu, M. Xu, et al., ChemSusChem 16 (2023) e202300736.
[6] P. Liu, N. Han, W. Wang, et al., Adv. Mater. 33 (2021) e2002582.
[7] H. Tsai, W. Nie, J.C. Blancon, et al., Nature 536 (2016) 312–316.
[8] W. Kong, F. Zeng, Z. Su, et al., Adv. Energy Mater. 12 (2022) 202704.
[9] J. Liang, Z. Zhang, Q. Xue, et al., Energy Environ. Sci. 15 (2022) 296–310.
[10] M. Shao, T. Bie, L. Yang, et al., Adv. Mater. 34 (2022) e2107211.
[11] C. Ma, M.F. Lo, C.S. Lee, et al., J. Mater. Chem. A 6 (2018) 18871–18876.
[12] J. Yan, W. Fu, X. Zhang, et al., Mater. Chem. Front. 2 (2018) 121–128.
[13] J. Shi, X. Jin, Y. Wu, et al., APL Mater. 8 (2020) 101102.
[14] L. Gao, F. Zhang, X. Chen, et al., Angew. Chem. Int. Ed. 58 (2019) 11737–11741.
[15] M. Long, T. Zhang, D. Chen, et al., ACS Energy Lett. 4 (2019) 1025–1033.
[16] J. Meng, D. Song, D. Huang, et al., Phys. Chem. Chem. Phys. 22 (2019) 54–61.
[17] R. Liu, H. Li, F. Zhang, et al., Solar Energy 209 (2020) 446–453.
[18] R. Liu, Y. Yu, C. Liu, et al., Sci. China Chem. 65 (2022) 2468–2475.
[19] R. Liu, Y. Yu, T. Hu, et al., J. Power Sources 512 (2021) 230452.
[20] S. Tan, N. Zhou, Y. Chen, et al., Adv. Energy Mater. 9 (2018) 1803024.
[21] Y. Yu, R. Liu, F. Zhang, et al., J. Colloid Interface Sci. 605 (2022) 710–717.
[22] D.H. Cao, C.C. Stoumpos, O.K. Farha, et al., J. Am. Chem. Soc. 137 (2015) 7843–7850.
[23] B. Traore, L. Pedesseau, L. Assam, et al., ACS Nano 12 (2018) 3321–3332.
[24] J. Zhang, H. Luo, W. Xie, et al., Nanoscale 10 (2018) 5617–5625.
[25] W. Chen, Y. Zhou, G. Chen, et al., Adv. Energy Mater. 9 (2019) 1803872.
[26] C. Bi, Q. Wang, Y. Shao, et al., Nat. Commun. 6 (2015) 7747.
[27] Y. Wang, J. Wu, P. Zhang, et al., Nano Energy 39 (2017) 616–625.
[28] L. Zhu, X. Zhang, M. Li, et al., Adv. Energy Mater. 11 (2021) 2100529.
[29] H. Yu, Y. Xie, J. Zhang, et al., Adv. Sci. 8 (2021) 2004510.
[30] Y. Yu, R. Liu, C. Liu, et al., Adv. Energy Mater. 12 (2022) 2201509.
[31] G. Wu, J. Zhou, J. Zhang, et al., Nano Energy 58 (2019) 706–714.
[32] H. Lai, D. Lu, Z. Xu, et al., Adv. Mater. 32 (2020) e2001470.
[33] X. Lian, H. Wu, L. Zuo, et al., Adv. Funct. Mater. 30 (2020) 2004188.
[34] W. Ke, C. Chen, I. Spanopoulos, et al., J. Am. Chem. Soc. 142 (2020) 15049–15057.
[35] D. Lu, G. Lv, Z. Xu, et al., J. Am. Chem. Soc. 142 (2020) 11114–11122.